RADIOXENON MEASUREMENTS WITH A COINCIDENCE SILICON DETECTOR SYSTEM

Wolfgang Hennig[1], Christopher E. Cox[1], Stephen J. Asztalos[1], Hui Tan[1], Patrick J. Franz[1], Ann Xiang[1], Peter M. Grudberg[1], William K. Warburton[1], Alan Huber[2], Steve Biegalski[3], Alex Brand[3], and Derek Haas[4]

XIA LLC[1], Amptek Inc[2], The University of Texas at Austin[3], and Pacific Northwest National Laboratory[4]

Sponsored by the National Nuclear Security Administration

Award No. DE-SC0004272 Phase II

ABSTRACT

The radioxenon detectors currently used in applications related to nuclear explosion monitoring have a very high sensitivity to detect very small amounts of radioxenon. However, to better distinguish the radioxenon background created by nuclear power plants and medical isotope facilities from a nuclear explosion, an improved discrimination of Xe isotopes is desirable. Silicon detectors have a number of advantages over the existing detectors (high resolution, low background, sensitivity to both photons and electrons, and no memory effect) and thus have the potential to outperform them in isotope discrimination.

In the work reported here, a radioxenon detector based on silicon PIN diodes has been designed, assembled, and tested. In Si-Si coincidence measurements with various Xe isotopes, resolutions were ~0.7 keV for 30 keV X-rays and 1.3-2.5 keV for conversion electrons at 129-232 keV. The presence of metastable Xe isotopes can easily be detected by observing conversion electron peaks in the energy spectra. The efficiency for detecting higher energy gamma rays is low, but backgrounds are practically zero so that overall the minimum detectable concentration is estimated to be well below 1 mBq/m^3 for a Si detector system with 100 mm^2 active area on each of the six sides of a cubic Xe cell.

OBJECTIVES

One of the tools used in nuclear explosion monitoring is the detection of atmospheric radioxenon. Existing radioxenon detectors, e.g., the SAUNA system (Ringbom et al., 2003), the PhosWatch detector (Hennig et al., 2009) and the SPALAX system (Fontaine et al., 2004), have a very high sensitivity to detect small amounts of radioxenon and can distinguish four key Xe isotopes. Because isotope ratios can be used to separate nuclear explosions from other sources like nuclear power plants and radiopharmaceutical facilities (Saey et al., 2010), better determination of isotope ratios emerges as a desirable feature in future developments. Besides generally improving the sensitivity (i.e., lowering the background or increasing the efficiency of the detector), distinction between isotopes can also be achieved by improving the detector's energy resolution so that key X-ray lines from the different isotopes no longer overlap in the energy spectra.

Silicon-based X-ray detectors such as silicon drift detectors (SDD) and PIN diodes have very high resolution at these X-ray lines. In addition, they can detect conversion electrons (CE) with high efficiency and excellent energy resolution, are sensitive to additional L X-rays, require no or simple cooling (with Peltier elements), show no memory effect, and have very low background even without lead shielding. Consequently, silicon based beta/X-ray coincidence detectors are a potential alternative to the existing scintillator based coincidence beta/gamma detectors or germanium based gamma only detectors.

In the work reported here, our objectives were to build a prototype of a silicon coincidence detector, test it with several Xe isotopes, and conduct a preliminary analysis of the data to estimate isotope activities.

RESEARCH ACCOMPLISHED

Si Detector System

In previously reported work (Cox et al., 2011, Hennig et al., 2011) we studied the response of Si detectors to electrons and photon at key Xe energies with test measurements and radiation transport simulations. It was concluded that both PIN diodes and SDDs are suitable for radioxenon detection, with the main difference that SDD achieve better resolution at higher temperatures and larger detector areas, but – at this time – with significantly higher cost. For our first prototype, we therefore chose to use PIN diodes with Peltier cooling. Two 25 mm^2 PIN diodes mounted on 1 cm^2 ceramic substrates were glued to two open sides of a ~1 cm^3 Cu cubic frame. A 1/16 inch stainless steel tube was attached on a third side, allowing evacuation of air and insertion of Xe. A two-stage Peltier cooler and mounting bracket was attached on a fourth side. The detector assembly and preamplifiers were mounted in an airtight box (5 × 4 × 10 cm^3 with feedthroughs for gas and electrical connections) and flushed with dry N_2 gas to prevent water condensation at an operating temperature of ~276 K. Pictures of the detector assembly are shown in Figures 1 and 2. The detectors were read out with an XIA xMAP spectrometer module, acquiring time-stamped list mode data from which coincidences were extracted offline.

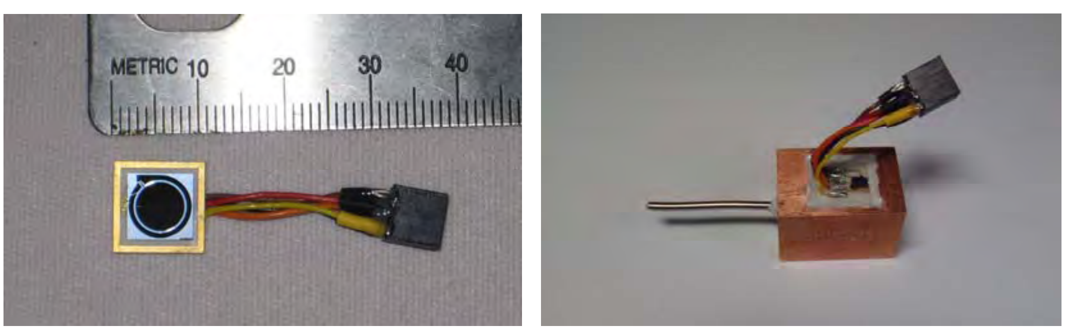

Figure 1. (Left) Picture of Si detector on ceramic substrate. (Right) Picture of Si detector glued into the copper cube acting as Xe cell (with filling tube)

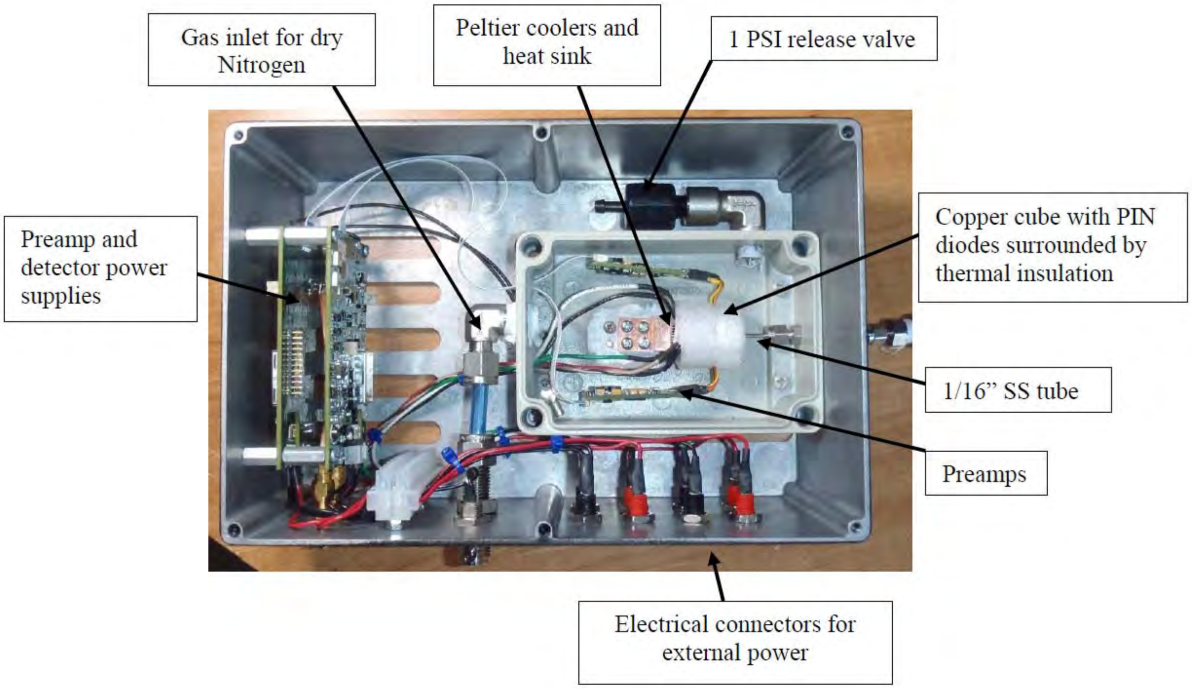

Figure 2. Picture of Si detector assembly. Inner box contains Si detector in foam wrapping, Xe filling tube to right, preamps above and below. Outer box contains HV and preamp power boards and associated wiring, as well as tubing for dry N_2 used to flush inner box from moisture.

Test Measurements

Figure 3 shows the energy spectra acquired in Xe measurements at the University of Texas at Austin, where a mixture of ^{133m}Xe and ^{133}Xe was obtained by the method of irradiating stable ^{132}Xe (Haas et al., 2009). The ^{133}Xe creates betas with energies up to 346 keV; ~4, 31, and 35 keV X-rays; 81 keV gamma-rays; ~25 keV Auger electrons; and 45 and 75-80 keV CEs, producing beta/CE, beta/X-ray, beta/gamma, and CE/X-ray coincidences. The ^{133m}Xe creates ~4, 30, and 34 keV X-rays; ~25 keV Auger electrons; and 199 and 228-233 keV CEs, producing CE/X-ray and CE/Auger coincidences. Coincidences with the variable energy beta absorbed in one detector and the fixed energy particle in the other detector form horizontal and vertical lines in the 2D spectrum. CE/X-ray coincidences from ^{133m}Xe form peaks at (4 keV/199 keV), (30 keV/199 keV), and (4 keV/228 keV). Auger/CE coincidences from ^{133m}Xe form a peak at (21 keV/199 keV), shifed from the nominal value by energy loss of the Auger electron in the Si dead layer and the Xe gas. Scattering of CEs from one detector to the other form diagonal lines with constant sum energy. As both detectors detect photons and electrons, the resulting spectrum is symmetric about the diagonal. Energy resolutions are listed in Table 1. At ≥30 keV, ^{133m}Xe coincidence peaks separate from the ^{133}Xe coincidence lines by the difference in their X-ray energies. The total count rate per detector was ~331 counts/s (~7 counts/s coincident). When the Xe was pumped out again, the total count rate was ~0.1 counts/s, (~0.001 counts/s coincident).

Figure 4 (left) shows the energy spectra acquired in ^{131m}Xe measurements at PNNL. Features are similar to ^{133m}Xe, only the CE energies are smaller. The total count rate per detector was ~22 counts/s (~0.32 counts/s coincident). Energy resolutions are listed in Table 1. A subsequent measurement with the Xe pumped out of the detector resulted in the background spectrum shown in Figure 4 (right). The total count rate per detector was ~0.2 counts/s (~0.0015 counts/s coincident). At the 159/4 keV peak, there were 0 counts in 24h, compared to ~500 counts in 16h in the Xe measurement.

The post-Xe measurements demonstrate the low background and neglible memory effect in Si detectors. We note that measured coincidence backgrounds (BG_{coinc}) are higher than expected from the simple assumption that BG_{coinc} is the product of the background in each detector and the coincidence window. For the PNNL measurement, the expected BG_{coinc} would be ~10^{-8} counts/s compared to the measured value of ~10^{-3} counts/s. Some of the additional background can be attributed to ^{125}I, a decay product of ^{125}Xe used in a previous test. With a new detector never exposed to internal sources, we obtain BG_{coinc} = 2.0×10^{-4} cps from a 1 week measurement (120 coincident counts). This is still higher than expected; further studies are under way to understand the source of this backgound and to develop possible ways of eliminating it.

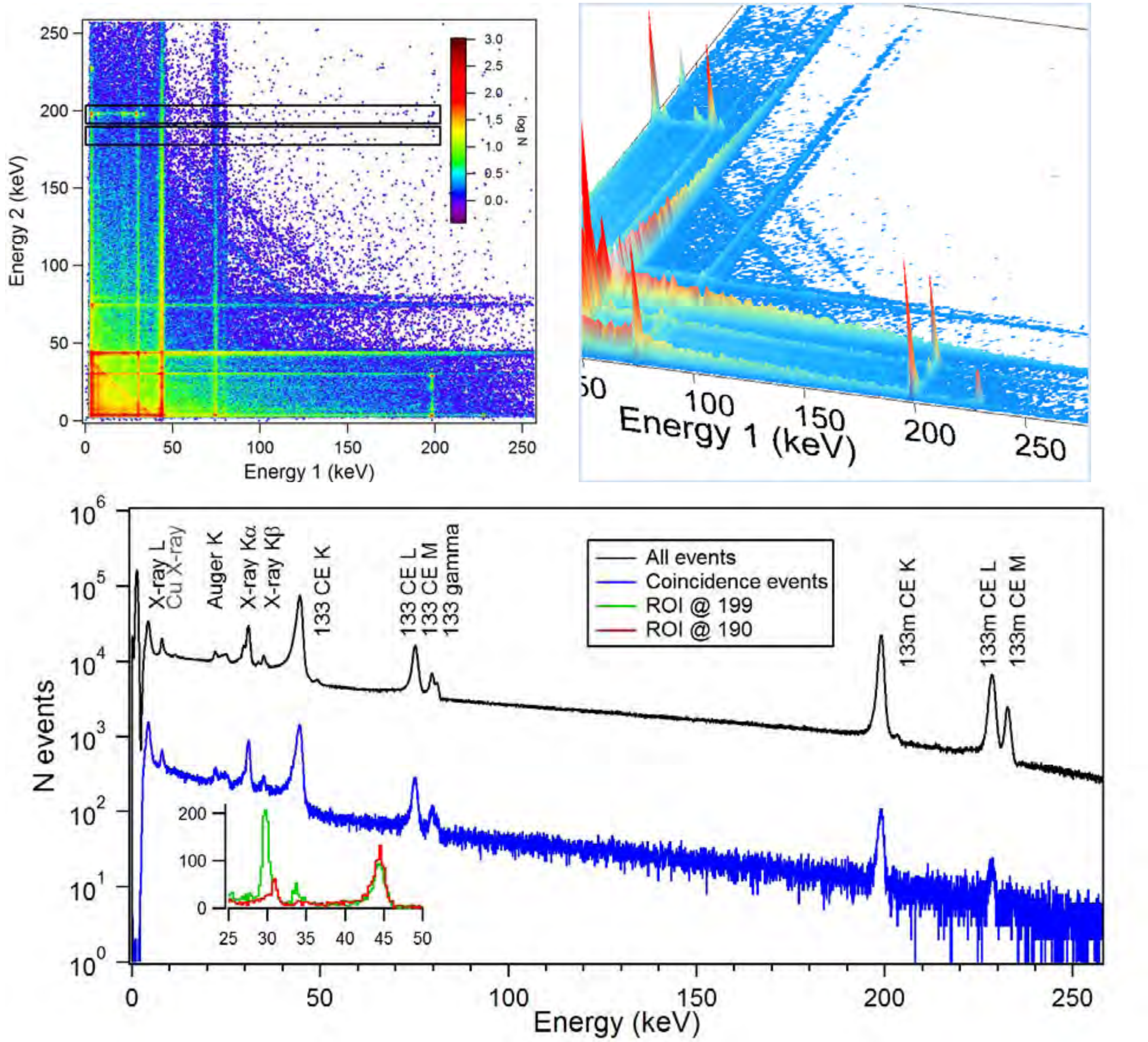

Figure 3. ^{133}Xe/^{133m}Xe energy spectra with Si prototype detector. Upper left: Conventional 2D plot colored by number of events in bin. Upper right: 3D surface plot of the same data, better visualizing the sharp CE peaks. Below: 1D histograms (projection to bottom axis) of all events and coincidence events of one detector. The inset shows the spectra from the ROI indicated by boxes in the 2D plot.

The resolution of the CE peaks varies in different measurements. In previous measurements at UT (Hennig et al., 2011), a single PIN test detector in a ~ 5 cm^3 cell made from Conflat vacuum flanges achieved better resolution than the current 1 cm^3 cell 2-PIN prototype. Both measurements used about the same amount of stable Xe for irradiation (about 0.56 cm^3), expanded into cell and manifold tubing. We attribute the lower resolution in 2012 to a) the higher gas pressure in the cell and/or b) small amounts of N_2 leaking into the cell from the surrounding box. In PNNL measurements, the Xe sample contained c) a "filler" of N_2 for better handling, which may have raised the pressure in the cell, and again there is a possibility of leaking. Since CE peaks are well separated, this peak broadening does not significantly affect the sensitivity of the detector. In fact, it can be used to estimate the amount of sample gas (if leaking is eliminated).

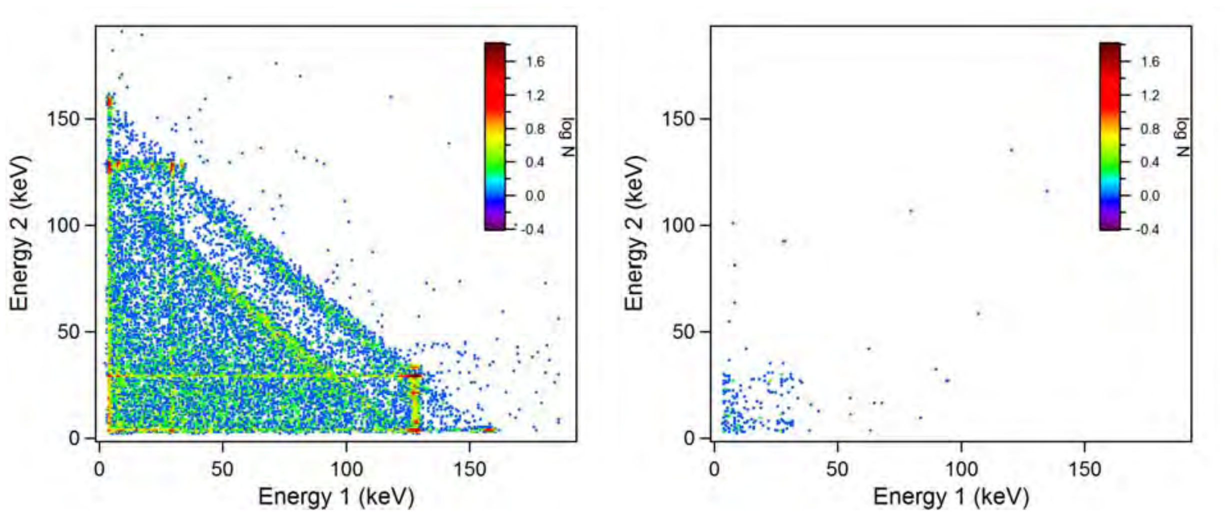

Figure 4: ^{131m}Xe spectrum (16h) and post ^{131m}Xe background (24h).

Table 1. Energy resolution in Xe measurements. UT 2011 measurements from (Hennig et al., 2011) used a single PIN (7 mm^2) test cell, UT 2012 and PNNL 2012 measurements used the 2-PIN prototype (25 mm^2 each).

Energy (keV)	Isotope / Particle	Measurement	Resolution (keV)	Comment
4	131m L Xray 133m/133 L Xray	PNNL 2012 UT 2012	0.75 1.0-1.1	doublet 2 doublets
30	133m K Xray	UT 2011 PNNL 2012 UT 2012	0.6 0.72 1.0	doublet
31	133 K Xray	UT 2011 UT 2012	0.6 0.8-0.9	doublet
45	133 K CE	UT 2011 UT 2012	0.99 1.5	
75	133 L CE	UT 2011 UT 2012	1.1 1.4	
129	133m K CE	PNNL 2012	3.1	
159	133m L CE	PNNL 2012	2.8	
199	133m K CE	UT 2011 UT 2012	1.14 1.3 - 1.6	
228	133m L CE	UT 2011 UT 2012	1.4 1.5-1.9	Several lines in peak

Preliminary Quantitative Analysis

To estimate activities from measured spectra, we developed a simple analysis routine that sums the counts in specific regions of interest (ROI) of the 1D histograms, factors in efficiencies, branching ratios, acquisition time and decay during acquisition, and returns the activity at the beginning of the measurement for each isotope. As this is intended for quick results only, only 2-3 ROIs per isotope are used, no effort is made to correct for coincidences or electrons interacting in more than one detector, and CE peaks are only corrected by subtracting an equivalent neighboring ROI of the ^{133}Xe beta continuum. No statistical errors or MDCs are computed at this time.

Detection efficiencies are taken from Monte Carlo simulations of the detector geometry used, see Figure 5 (left). The detector was modeled as a pure Cu block with overall dimensions of 1.4 × 1.4 × 2.0 cm^3 with 1.1 × 1.1 cm^2 openings for SiO_2 substrates. Two 25 mm^2 PIN detectors 0.45 mm thick and 1.0 cm apart were placed at the center of opposing SiO_2 substrates with Xe gas at STP uniformly filling the detector volume. A million events were simulated for each of several key energies and particles. The detection efficiency was defined as the number of events that deposited full energy versus the total number of simulated particles. An energy spectrum of 199 keV electrons interacting with a single PIN diode is shown in Figure 5 (right). The *full* energy efficiencies for electrons depend only slightly on the energy and are 3.1-3.3% for 45-199 keV (~6.5% for interactions depositing *any* energy), compared to a geometric active area fraction of 4.2%. *Full* energy efficiencies for photons are 3.7%, 0.5% and ~0.025% at 4 keV, 30 keV and 81 keV, respectively.

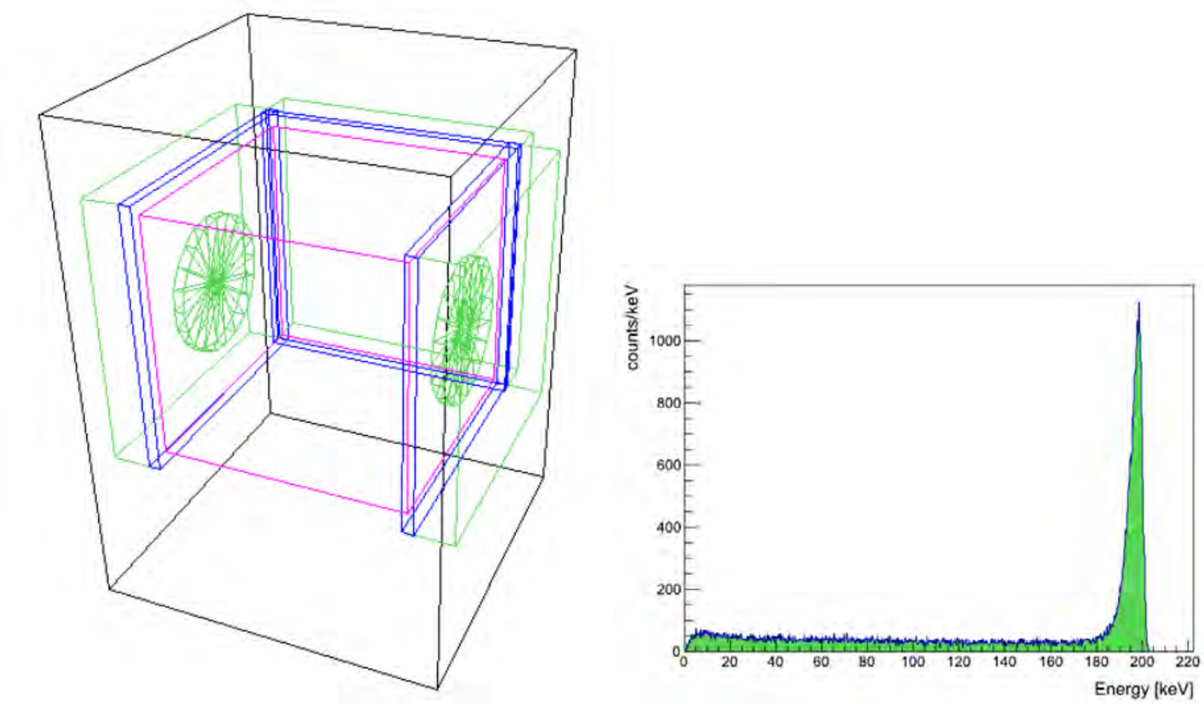

Figure 5. (Left) Side view of the PIN diode detector geometry used for efficiency simulations. Black defines the Cu body, magenta the Xe cell (interior), blue the SiO^2 wafers and hatched green the 25 mm^2 PIN diodes. (Right) Simulated energy spectrum of 199 keV conversion electrons uniformly emitted within the Xe volume.

Table 2 summarizes the analysis results for the Xe and background measurements at UT and PNNL. Activities computed from different ROIs agree well. The data shown in Table 2 are consistent with the expected activities of the sample from irradiation, assuming a 15% transfer efficiency between the created sample and detector cell. This is reasonable considering the volumetric differences and the losses in the transfer lines in the test setup. The ^{133m}Xe/^{133}Xe ratio is also commensurate with the expected value. Figure 6 shows the radioxenon activities as a function of time for the measured sample.

Table 2. Net Counts in 1D ROIs and corresponding activity (in mBq) at start of measurement. Bold fields indicate the major isotopes in each Xe sample.

Isotope	ROI (keV)	Net counts UT 2012	Activity UT 2012	Net counts PNNL 2012	Activity PNNL 2012	Net counts PNNL 2012 background	Activity PNNL 2012 background
131m	129 158-163	-2,441 4,699	-1k 6k	**289,755** **191,979**	**267k** **286k**	22 30	0 0
133m	199 228 232-233	**642,213** **210,611** **46,221**	**567k** **559k** **548k**	-9 50 -7	0 0 0	5 -8 6	0 0 0
133g	45 75	**2,093,114** **346,155**	**2,157k** **2,354k**	5050 273	5k 1k	-72 6	0 0

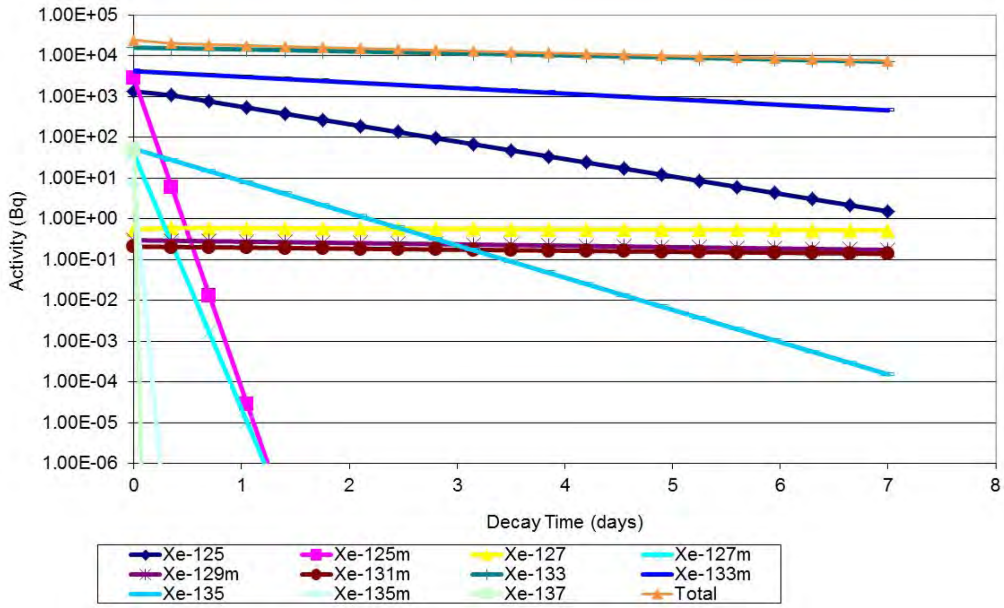

Figure 6. Radioxenon activites as a function of decay time for 0.56 cm^3 enriched (99.9%) ^{133}Xe sample (100 kW for 1 hour in UT TRIGA reactor).

With a large number of ROIs, including overlapping ROIs for beta isotopes and metastables at 4 keV, the above analysis is tedious and error prone. Future analysis with employ the Spectral Deconvolution Analysis Tool (SDAT) analysis tool (Biegalski et al., 2008). SDAT utilizes the standard spectrum method for spectrum analysis where the contribution of each radionuclide is fit within the spectrum. Library vectors containing pure spectra of the following six components are necessary for radioxenon analysis: ^{131m}Xe, ^{133m}Xe, ^{133}Xe, ^{135}Xe, radon, and detector background. The library vectors are fit to the sample spectrum via a least-squares algorithm to determine the magnitude of each spectral component. SDAT was developed for the analysis of β-γ coincidence spectra from detectors with BC-404 plastic scintillators as the β detector. Adaptations of the tool are now in progress at UT Austin so that spectra from the coincidence Si detector may be utilized.

Estimated Sensitivity

Using backgrounds and energy resolution from test measurements and detector efficiencies from simulations, we previously estimated the minimum detectable concentration (MDC) for the four Xe isotopes of interest (Hennig et al., 2011). Simplifying the definition in (Ringbom et al., 2003), as described in (Hennig et al., 2012) we approximate MDC as

$$MDC = (2.71 + 4.65\,\sigma) / (\varepsilon_{\beta\gamma} \times \beta\gamma \times t_{acq} \times V) \qquad (1)$$

Where σ^2 is the number of measured background counts in an ROI, $\varepsilon_{\beta\gamma}$ is the coincidence detection efficiency for the ROI, $\beta\gamma$ is the branching ratio into the ROI from literature (Browne and Firestone, 1986), V is the collected air volume, and t_{acq} is the measurement time, assumed to be 24 h. In the case of multiple ROIs, the background σ and product $\varepsilon_{\beta\gamma} \times \beta\gamma$ are replaced by their sums over the individual ROIs. For the specific case of two ROIs, Equation 1 becomes

$$MDC = (2.71 + 4.65\,\sigma_t) / ((\varepsilon_{\beta\gamma 1} \times \beta\gamma_1 + \varepsilon_{\beta\gamma 2} \times \beta\gamma_2) \times t_{acq} \times V) \qquad (2)$$

Where σ_t^2 equals $\sigma_1^2 + \sigma_2^2$ - the sum in quadrature of measured background counts in each ROI. For ROI 1, the coincidence detection efficiency is $\varepsilon_{\beta\gamma 1}$ and the branching ratio $\beta\gamma_1$, with 1→ 2 for ROI 2. Since backgrounds are extremely low, the numerator is generally dominated by the term 2.71. Selected results are listed in Table 3, column 3. The detector geometries are as follows (keeping the previous enumeration):

Detector B—A 1 cm^3 cube with a single Si detector (25 mm^2 active area) in each of two active sides. This geometry has two coincidence permutations (electron left, photon right, and vice versa).

Detector C—Same as B but 100 mm^2 detectors in all six sides of the cube (30 coincidence permutations).

Detector D—A 5 cm^3 cube with four Si detectors (25 mm^2 active area each) in each of its six sides (552 coincidence permutations).

Detector B represents the geometry of the prototype. Detectors C and D are examples of high efficiency detectors: Detector C is the ideal case with very large PIN diodes or SDDs and no dead area, which is included for illustration but at current state of the art suffers either from bad resolution (with large PINs) or high cost (with large SDD). Detector D models the geometry of our proposed next prototype, using arrays with four 25 mm^2 PINs on a common 1.7cm x1.7cm substrate with an active area fraction of ~34%.

Following the Xe measurements described above, we can refine the previous MDC estimates in a number of ways: First, from Figure 3 we can see that there are a significant number of ^{133}Xe beta/CE and X-ray/CE coincidences detected at 45 keV and 75 keV, which have not been included in the previously estimated MDC for ^{133}Xe. Adding beta/CE and X-ray/CE ROIs into the MDC calculation and adjusting all ROIs for measured resolutions, we obtain the MDCs in column 4, improved by a factor of about 4-10 for the beta emitter isotopes. The improvement is due to the relatively high value of $\varepsilon_{\beta\gamma} \times \beta\gamma$ for beta/CE coincidences: the combined product for ^{133}Xe ROIs is ~10% for X-ray/beta coincidences, ~7.4% for X-ray/CE coincidences and ~46% for beta/CE coincidences (not including the detector specific active area fraction) For ^{135}Xe, the combined products are ~0.5% for X-ray/beta coincidences, ~0.4% for X-ray/CE coincidences and ~4.1% for beta/CE coincidences. Use of Auger/CE coincidences may further improve the MDC, but are difficult to count due to their low energy and consequent relatively high energy loss in the gas and the Si dead layer.

Second, we previously disregarded cross contamination from isotopes with beta decays into the CE ROIs of metastable isotopes, assuming they can be separated by the X-ray energy. From Figure 3 we can see that this assumption is just about correct for 30/31 keV K X-rays, but not for ~4 keV L X-rays. Assuming a (substantial) ^{133}Xe concentration of 100 mBq/m^3, 10% ROI overlap at 30 keV and 100% ROI overlap at 4 keV, we can compute the number of beta/X-ray coincidences that will fall into the ROIs of metastable isotopes and thus increase the background term. The MDC of metastable isotopes then increases to about 1 mBq/m^3 for the high efficiency detectors (column 5). However, this beta cross contamination can be further suppressed by excluding triple coincidences from the ROI in a system with 3 or more detectors. For example, a ^{133}Xe beta decay followed by a 75 keV CE and 4 keV X-ray may create a count in the ^{133m}Xe ROI at (199 keV/4 keV) if only a beta and X-ray are detected. However, if a third detector detects the 75 keV CE at the same time, it is clear that the event comes from ^{133}Xe and the count can be removed from the ^{133m}Xe ROI. This would reduce the cross contamination by as much as 31% and 66% for detectors B and C (depending on the number of PIN diodes and active area) and thus lower the MDCs listed in column 5. An additional, but smaller suppression of beta background comes from events where CE and X-ray hit the same detector and from events with higher number of particles (e.g., beta + 45 keV CE + 30 keV

X-ray + 4 keV X-ray). Cross contamination of decays from ^{131m}Xe and ^{133m}Xe into ^{133}Xe ROIs is not considered here because the metastables' CE peaks are sufficiently narrow to simply exclude them from ^{133}Xe ROIs.

Third, as noticed above, measured coincidence backgrounds do not agree with our assumption of coincidence background being the product of individual backgrounds and the coincidence window. Using the measured average coincidence background of the uncontaminated detector, we obtain the slightly increased values in column 6. However, this measured background has a very large uncertainty; the measured coincidence background in a particular ROI is often zero. These results are therefore best understood as an upper limit. As noted above, sources and/or removal of this unexpected background are under investigation.

Overall, the estimated MDCs for the high efficiency detectors are typically well below 1 mBq/m^3, which is the requirement for ^{133}Xe detection in IMS monitoring stations. Existing detectors reach between 0.1 and 1 mBq/m^3 in the absence of large memory effects (Bowyer et al., 2011, Hennig et al., 2009, Fontaine et al., 2004).

When distinguishing nuclear explosions from other sources of atmospheric radioxenon, one often employed method is to plot measured isotope ratios and compare them to a "separation line" (Kalinowski et al., 2010). A sample of radioxenon with an initial ratio of isotopes will not cross this line as the isotopes decay over time. Typically a 4-isotope plot is used, which has the advantage that explosions fall on one side of the separation line and all other sources fall on the other. On a 3-isotope plot, a subset of the "other" sources may fall on the "explosion" side of the plot, in an area corresponding to an explosion that has decayed for some time T_D. For ^{135}Xe, CE and X-ray branching ratios are small, which means that Si detectors have lower sensitivity for ^{135}Xe than for the other isotopes – the MDC is about a factor 10 higher (though still in the range of 0.2-2 mBq/m^3). Therefore 4-isotope plots may not be applicable. However, since a) ^{135}Xe is rarely detected from a location not close to an IMS station and b) the time limit T_D is in the order of 50 days for a 3-isotope plot without ^{135}Xe, we believe there is not a significant loss of sensitivity for using only ^{131m}Xe, ^{133}Xe, and ^{133m}Xe for source discrimination with Si detectors.

Table 3. Estimated MDC for Xe isotopes (in mBq/m^3)

Isotope	Detector	Previous estimate (Using X-ray/CE for metatsable isotopes and only X-ray/beta for beta emitters)	Adding CE/beta and X-ray/CE ROIs for beta emitters	With beta cross-contamination (100mBq/m^3 ^{133}Xe) and CE/beta and , X-ray/CE ROIs	Using measured coincidence background and CE/beta and X-ray/CE ROIs
131m	B (2 PIN) C (6 SDD) D (24 PIN)	25.32 0.11 0.16	No change	38.50 0.96 1.20	25.51 0.12 0.17
133m	B C D	23.08 0.10 0.15	No change	35.09 0.87 1.10	23.25 0.11 0.15
133g	B C D	22.28 0.09 0.14	4.04 0.02 0.03	No change	4.60 0.05 0.05
135g	B C D	439.42 1.83 2.75	45.41 0.19 0.29	Not calculated	52.39 0.64 0.53

CONCLUSIONS AND RECOMMENDATIONS

In summary, we built a 2-PIN prototype Si detector for radioxenon detection, tested it with Xe samples, and developed a preliminary quantitative analysis routine. Si detection efficiencies for Xe gamma rays are low, but energy resolutions for X-rays and CE are high and backgrounds are extremely low. With multiple detectors, all sensitive to betas, CEs and photons, Si based detectors can make use of beta/CE coincidences in addition to the photon/beta and photon/CE coincidences employed in existing scintillator based detectors, which increases sensitivity. From the test measurements, upper limits for any Xe memory effect range from 1:3000 to 0:500, i.e., there is practically no memory effect.

In ongoing work, we are building a high efficiency Si detector, consisting of 24 PIN diodes for a total of 100 mm^2 active area on each of the six sides of a cubic Xe cell. The basic mechanical design of this detector is complete, with improved vacuum-tightness to eliminate leaking, and its cooling mechanism has been tested successfully. A custom arrangement of four 25 mm^2 PIN diodes on a common substrate has been designed and is about to be manufactured. The MDC of this detector is estimated to be well below 1 mBq/m^3.

Si detectors thus meet several key requirements for detectors in radioxenon monitoring stations. With their lower complexity, no need for lead shielding, and the ability to detect ^{37}Ar L X-rays in the same detector, they may also be a good match for on-site inspection applications.

REFERENCES

Biegalski KMF, Biegalski SR, and Haas D (2008) Performance Evaluation of Spectral Deconvolution Analysis Tool (β) Software Used for Nuclear Explosion Radionuclide Measurements, *J. Radioanal. Nuc. Chem.* **276**(2), 407–413.

Bowyer T.W., S.R. Biegalski, M.W. Cooper, P.W. Eslinger, D. Haas, J.C. Hayes, H.S. Miley, D.J. Strom, and V.Woods (2011). Elevated radioxenon detected remotely following the Fukushima nuclear accident. *J. Environ. Radioact.* **102**, 681–687.

Browne, E. and R. Firestone (1986). *Table of Radioactive Isotopes*, J. Wiley.

Cox C.E., S.J. Asztalos, W. Hennig, and W.K. Warburton (2011). Electron response in windowless Si(Li), SDD and PIN diode photodetectors *Proceedings of the 2011 IEEE Nuclear Science Symp*, 2074–2080 (paper ID NS45-4).

Fontaine, J-P., F. Pointurier, X. Blanchard, and T. Taffary (2004). Atmospheric xenon radioactive isotope monitoring, *J. Environ. Radioact.* **72**, 129.

Haas, D.A., S.R. Biegalski, and K.M. Foltz Biegalski (2009). Radioxenon production through neutron irradiation of stable xenon gas, *J Radioanal Nucl Chem* **282**, 677–680.

Hennig, W., W. K. Warburton, A. Fallu-Labruyere, K. Sabourov, M. W. Cooper, J. I. McIntyre, A. Gleyzer, M. Bean, E. P. Korpach, K. Ungar, W. Zhang, and P. Mekarski (2009). Development of phoswich detector system for radioxenon monitoring, *J. Radioanal. Nucl. Chem.* **282**, 681.

Hennig, W., C. E. Cox, S. J. Asztalos, H. Tan, P. J. Franz, P. M. Grudberg, and W. K. Warburton (2011). Study of silicon detectors for high-resolutin radioxenon measurements, in *Proceedings of 2011 Monitoring Research Review: Ground-Based Nuclear Explosion Monitoring Technologies,* LA-UR-11-04823, Vol. 2, pp. 695–707.

Hennig, W., C. E. Cox, S. J. Asztalos, H. Tan, P. J. Franz, P. M. Grudberg, W. K. Warburton and A. Huber (2012). submitted to *J Radioanal Nucl Chem.*

Ringbom, A., T. Larson, A. Axelson, K. Elmgren, and C. Johansson (2003). SAUNA—A system for automatic sampling, processing and analysis of radioactive xenon, *Nucl. Instrum. Methods Phys. Res., Sect. A* **508**: 542–553.

Saey P.R.J, T.W. Bowyer, A. Ringbom (2010). Isotopic noble gas signatures released from medical isotope production facilities—Simulations and measurements. *Appl. Rad. And Isotopes* **68** (9), 1846–1854.